

Iron abundances from optical Fe III absorption lines in B-type stellar spectra

H. M. A. Thompson^{1*}, F. P. Keenan¹, P. L. Dufton¹, C. Trundle¹, R. S. I. Ryans¹ and P. A. Crowther²

¹*Astrophysics Research Centre, School of Mathematics and Physics, Queen's University, Belfast BT7 1NN*

²*Department of Physics and Astronomy, University of Sheffield, Hicks Building, Hounsfield Rd, Sheffield, S3 7RH*

Accepted Received in original form

ABSTRACT

The role of optical Fe III absorption lines in B-type stars as iron abundance diagnostics is considered. To date, ultraviolet Fe lines have been widely used in B-type stars, although line blending can severely hinder their diagnostic power. Using optical spectra, covering a wavelength range $\sim 3560 - 9200 \text{ \AA}$, a sample of Galactic B-type main-sequence and supergiant stars of spectral types B0.5 to B7 are investigated. A comparison of the observed Fe III spectra of supergiants, and those predicted from the model atmosphere codes TLUSTY (plane-parallel, non-LTE), with spectra generated using SYNSPEC (LTE), and CMFGEN (spherical, non-LTE), reveal that non-LTE effects appear small. In addition, a sample of main-sequence and supergiant objects, observed with FEROS, reveal LTE abundance estimates consistent with the Galactic environment and previous optical studies. Based on the present study, we list a number of Fe III transitions which we recommend for estimating the iron abundance from early B-type stellar spectra.

Key words: atomic data – line: identification – Galaxy: abundances – stars: abundances – (stars:) supergiants – stars: variables: other

1 INTRODUCTION

Iron lines dominate the spectra of many astrophysical objects, such as novae (McKenna et al. 1997; Hatzidimitriou et al. 2007), photoionized H II regions (Rubin et al. 1997; Rodríguez 2002; Esteban et al. 2002) and active galactic nuclei (Sigut & Pradhan 2003; Sigut, Pradhan & Nahar 2004; Zhang, Dultzin-Hacyan & Wang 2007). The atomic processes for iron and other iron-group ions have been the subject of numerous investigations, for example the IRON Project (Hummer et al. 1993) which considers applications in astrophysical and laboratory plasmas (Pradhan et al. 1996). Absorption lines of iron provide important metallicity diagnostics for both stars and galaxies, and also play a key role in investigating star formation histories through element ratios, such as $[\alpha/\text{Fe}]$ (Gilmore & Wyse 1998). However, there is a lack of robust Fe abundance

determinations in external galaxies, e.g. the Magellanic Clouds (see for example, Rolleston, Trundle & Dufton 2002; Trundle et al. 2002, 2007 and Mokiem et al. 2007), due to the complex Grotian diagrams for Fe, the low metallicity environment of the Magellanic Clouds and the reliability of the currently available atomic data.

Early B-type stars are important for studying the chemical composition of our own and other galaxies (Kilian 1992; Dufton 1998). In the optical spectra of B-type stars, iron lines due to a number of ionization stages are observed (see for example, Gies & Lambert 1992; Lennon, Dufton & Fitzsimmons 1993; Smartt, Dufton & Lennon 1997; Morel et al. 2006). Absorption features arising from Fe III are primarily detected (Hardorp & Scholz 1970), with Fe II also found in later B-type stars (Pintado & Adelman 1993). Fe IV lines are not expected in the optical spectra of B-type stars due to their intrinsic weakness in this temperature range.

The optical Fe III line spectrum has not been widely employed to determine abundances, as it has often been believed to be too weak to provide reliable measurements (Kendall et al. 1994a). However, it has been used for chemical composition studies of several bright, narrow-

* email: h.thompson@qub.ac.uk

Based on observations made with the WHT operated on the island of La Palma by the Isaac Newton Group in the Spanish Observatorio del Roque de los Muchachos of the Instituto de Astrofísica de Canarias

lined main-sequence B-type stars, such as ζ Cas, γ Peg, ι Her, τ Sco and λ Lep (Snijders 1969; Peters & Aller 1970; Hardorp & Scholz 1970; Peters 1976; Peters & Polidan 1985). These Galactic objects have sufficiently high Fe content, coupled with narrow metal absorption lines (due to their low projected rotational velocities), so that, even with relatively poor quality optical spectra, Fe III features can be detected. However, the quality of the available spectra did not allow the study of Fe III lines in objects of lower metallicity. Therefore, more recently the optical wavelength range has been largely overlooked in favour of the ultraviolet domain (Swings & Vreux 1976; Peters & Polidan 1985; Dixon & Hurwitz 1998), and in particular the very rich spectral region around 1900 Å (Thompson, Humphries & Nandy 1974; Heber 1983; Kendall et al. 1994a; Grigsby, Mulliss & Baer 1996; Moehler et al. 1998). On the other hand, due to the high density of absorption features and resultant blending, continuum placement in the ultraviolet is difficult, and hence significant errors may be present in the derived abundances (Moehler et al. 1998).

Due to instrumental advances in more recent years, it has become routine to obtain high resolution and signal-to-noise (S/N) spectra, and the use of the optical Fe III lines as a diagnostic has been revisited (e.g. Cunha & Lambert 1994; Kilian 1994). A number of main-sequence objects have subsequently been re-examined, for example γ Peg and ι Her (Pintado & Adelman 1993; Liu, Sterken and Zhao 1998), producing results consistent with the earlier optical analyses. In addition, the higher S/N ratios of the available spectra have made it possible to detect the weak optical Fe III lines in a number of lower metallicity objects, such as AV 304 in the Small Magellanic Cloud (Rolleston et al. 2003), and the globular cluster post-AGB stars ZNG-1 in M 10 (Mooney et al. 2004), Barnard 29 in M 13 and ROA 5701 in ω Cen (Thompson et al. 2007).

A number of B-type stars have been studied using both ultraviolet and optical spectra, but the corresponding abundance estimates are generally in poor agreement. Estimates from the ultraviolet spectra are consistently lower than those from the optical, for example in the post-AGB stars Barnard 29, ROA 5701 (Thompson et al. 2007), BD +33°2642 (Napiwotzki, Heber & Köppen 1994) and HD 177566 (Kendall et al. 1994a,b). Young Galactic objects including γ Peg (Moehler et al. 1998) and ι Her (Grigsby et al. 1996), plus stars in known metallicity environments such as the Magellanic Clouds (Dufton et al. 2007), also display similar discrepancies.

Here, high resolution spectra for a number of narrow-lined Galactic B-type main-sequence and supergiant stars, covering a range of spectral types, are analysed using LTE and non-LTE model atmosphere techniques. Details on the observations, models and Fe III line selection can be found in Sections 2 and 3. An LTE approximation is considered, and the reliability of such an assumption, along with an assessment of the individual Fe III lines, is discussed in Section 4.

2 OBSERVATIONS AND DATA REDUCTION

The observational data included here are used for two investigations. Firstly, to allow a comparison between the TLUSTY (Hubeny 1988; Hubeny & Lanz 1995; Hubeny, Heap & Lanz 1998) and CMFGEN (Hillier et al. 2003) model atmosphere codes, and secondly, an investigation of the reliability of the Fe III spectrum to estimate abundances. The first investigation utilizes a subset of the stars discussed in Crowther, Lennon & Walborn (2006) for which there were suitable data from ISIS/WHT and FEROS/ESO, and these objects are listed in Table 1. Crowther et al. (2006) analysed a sample of 25 Galactic B-type supergiants using optical spectra from three sources; CTIO data obtained using the Loral 1K spectrograph, WHT spectra taken using the ISIS spectrograph (Smartt, private communication) and JKT spectra from the Richardson-Brealey spectrograph (Lennon, Dufton & Fitzsimmons 1992). A number of objects were omitted from this study due to having poorly detected or unseen Fe III features (i.e. objects of spectral type B0.5 and earlier), or if their atmospheric parameters lay outside the available TLUSTY grid points (for example, HD 13854, HD 152236, HD 190603 and HD 194279). For the second investigation, a sample of B-type stars, consisting of two main-sequence stars and nine supergiants, has been selected, from a FEROS/ESO dataset. These are analysed using the TLUSTY atmosphere code and are listed in Table 2. The objects have been chosen to cover a range of spectral types and have relatively narrow-lined absorption spectra. The supergiant HD 53138 has been included in both samples due to it having a rich Fe III line spectrum.

The WHT data were taken using the Intermediate-dispersion Spectrograph and Imaging System (ISIS), on 1999 July 08. The EEV12 CCD detector (2148×4200 pixels) was used on the blue arm with the R1200 grating and a slit width of 1.0 arcsec. This resulted in a wavelength coverage of \sim 3920–4720 Å. Typical S/N values for spectra at \sim 4500 Å are given in Table 1. The data were reduced using standard procedures within IRAF, which included flat-fielding, bias subtraction and wavelength calibration and the combined spectra read into the Starlink package DIPSO (Howarth et al. 2004) for further analysis.

High resolution ESO spectra were obtained using the Fiber fed Extended Range Optical Spectrograph (FEROS, Kaufer et al. 1999), between 2005 April 21 and 24 (proposal 075.D-0103(A)). The EV 2K×4K CCD detector and 79 lines mm^{-1} échelle grating were used, resulting in a spectral resolution of $R \sim$ 48000 and a wavelength coverage of \sim 3560–9200 Å. Data were reduced using the standard FEROS Data Reduction System (DRS), implemented with ESO-MIDAS software. The reduced spectra for a given target were subsequently combined using SCOMBINE within IRAF¹, and imported into DIPSO for further analysis. Their average S/N ratios at \sim 4500 Å are given in Tables 1 and 2.

The spectra were normalised with low-order polynomials and radial velocity shifted to the rest frame using unblended metal and hydrogen lines. Absorption line equiv-

¹ IRAF is distributed by the National Optical Astronomy Observatories, which are operated by the Association of Universities for Research in Astronomy, Inc., under cooperative agreement with the National Science Foundation.

alent widths were estimated by fitting Gaussian profiles to the lines. The error in measuring these is discussed in Dufton et al. (1990), with a well-observed unblended feature accurate to 10 per cent (designated ‘a’ in Tables 4, 5 and 6), weak or blended features accurate to 20 per cent (designated ‘b’) and weaker features accurate to less than 20 per cent (designated ‘c’).

3 DATA ANALYSIS

3.1 Model atmosphere techniques

Two model atmosphere codes have been used in this paper, namely TLUSTY and CMFGEN, which are discussed below.

Non-LTE model atmosphere grids, calculated with TLUSTY and SYNSPEC (Hubeny 1988; Hubeny & Lanz 1995; Hubeny et al. 1998), have been used to derive atmospheric parameters. The methods involved are discussed in, for example, Ryans et al. (2003), Hunter et al. (2005), Thompson et al. (2006, 2007) and Trundle et al. (2007), whilst greater detail about the grids may be found in Dufton et al. (2005) and at <http://star.pst.qub.ac.uk>. Briefly, four grids were calculated corresponding to the Galaxy, the Large (LMC) and Small (SMC) Magellanic Clouds and a lower metallicity regime. The Galactic grid has been adopted throughout this analysis and covered a range of effective temperatures (12000 to 35000 K), logarithmic gravities ($\log g = 4.5$ dex down to the Eddington limit; g in cm s^{-2}) and microturbulences ($\xi = 0, 5, 10, 20$ and 30 km s^{-1}). Typical spacing between grid points for the effective temperature and surface gravities were 2500 K and 0.25 dex, respectively. For accurate profile fitting of the hydrogen lines, further models were executed at a resolution of 0.1 dex for $\log g$, with these models used only in determining the surface gravity. The metal line blanketing was assumed to be dominated by iron, with the exclusion of nickel in our models unlikely to be a source of significant error in the atmospheric parameters and chemical composition (Hubeny et al. 1998).

Iron is included in the non-LTE TLUSTY model atmosphere calculations with sets of ionic levels being collected into superlevels in order to make the calculations tractable. Although in the spectral synthesis code it is possible to assign ionic levels to appropriate superlevels, we have instead opted to calculate the Fe III spectrum in an LTE approximation. These were then employed with the measured equivalent widths to derive the abundance estimates shown in Tables 4, 5 and 6 (see Thompson et al. 2007). Atomic data for the Fe III lines were taken from Nahar & Pradhan (1996), as these are (to our knowledge) the most up-to-date values available. Their oscillator strengths are shown in Table 3 (available in full on-line), along with those from the Kurucz database (<http://nova.astro.umd.edu>, Hubeny 1988; Hubeny & Lanz 1995; Hubeny et al. 1998), plus the wavelength, transition, and g_i and g_j values for the selected iron lines.

The TLUSTY model atmosphere grids are based upon the standard solar composition (Grevesse & Sauval 1998), while SYNSPEC allowed a range of iron abundances to be calculated. Thus, using the Galactic grid, spectra were synthesised for a range of iron abundances from 6.7 and 8.3 dex. Dufton et al. (2007) discuss the possible inconsistencies which can arise from the adopted abundances used in

both the model atmosphere and spectrum synthesis calculations, i.e. the use of SYNPLLOT to synthesize spectra for a range of metallicities which differ from that of the underlying model atmosphere calculation. Tests discussed by Dufton et al. (2007) indicate that these should not be a significant source of error, and the method has been widely used (see for example Kilian 1994; McErlean, Lennon & Dufton 1999 and Korn et al. 2000).

CMFGEN is a non-LTE line blanketed multi-purpose atmospheric code designed for the spectral analysis of stars with stellar winds. It solves the radiative transfer equation for spherical geometry in the co-moving frame, under the constraints of statistical and radiative equilibrium (Hillier & Miller 1998). As CMFGEN does not solve the momentum equation, the mass-loss rate and velocity law must be specified.

Crowther et al. (2006) used the current version of CMFGEN (Hillier et al. 2003) and again adopted the atomic data of Nahar & Pradhan (1996) for the Fe III lines. A model similar to that applied by Evans et al. (2004) was used by Crowther et al. (2006), comprising 26 ions of H, He, C, N, O, Mg, Al, Si, S, Ca and Fe for early B subtypes, containing a total of 2636 individual levels which were grouped into 766 superlevels, with a full array of 25960 bound-bound transitions. Higher ionization stages were excluded for spectral types B2.5 and B3. The temperature structure was determined by radiative equilibrium, with the velocity parameterized with a classical β -type law for the supersonic part (with the exponent in the range $\beta = 1 - 3$, selected on the basis of the $H\alpha$ profile), and the subsonic velocity set by the corresponding H-He TLUSTY photospheric models calculated for each CMFGEN model atmosphere calculation (Hillier & Lanz 2001). Test calculations have been performed for a H-He TLUSTY photospheric model and a blanketed TLUSTY model (Dr. S. Searle, private communication). The results showed comparable stellar parameters, and hence the use of the H-He TLUSTY model here appears valid for this analysis. Synthetic spectra for each star were obtained for iron abundances of Fe = 7.35, 7.65 and 7.95 dex, adopting the appropriate atmospheric parameters. These were used to derive the abundance estimates given in Table 4 (see Section 3.3 for further details).

3.2 Atmospheric parameters

The atmospheric parameters of the objects used in the comparison between the model atmosphere codes CMFGEN and TLUSTY are listed in Table 1. Table 2 contains the atmospheric parameters of the additional objects which have been analysed solely with TLUSTY.

Crowther et al. (2006) used the non-LTE model atmosphere code CMFGEN to deduce the atmospheric parameters listed in Table 1. They estimated surface gravities at individual temperatures for a second order $\log g - T_{\text{eff}}$ fit based on previous studies of B-type supergiants. An initial $\xi = 20 \text{ km s}^{-1}$ was assumed, with values considered in the range of $10 - 40 \text{ km s}^{-1}$ in multiples of 5 km s^{-1} , if the fits of helium and silicon lines were not in agreement. Values of the projected rotational velocity ($v \sin i$) were taken from Howarth et al. (1997), with the exception of HD 14956 which was not included in their sample. For their temperature estimate, Crowther et al. (2006) employed the silicon

Table 1. Adopted atmospheric parameters for the sample of supergiants employed in the comparison between the model atmosphere calculations using CMFGEN and TLUSTY. The spectral types and CMFGEN parameters are taken from Crowther et al. (2006), with additional spectral types from Lennon et al. (1992)^a. Note that the atmospheric parameters derived from the two codes have, in general, been determined using different data sets (D[†]).

HD Number	Name	Spectral Type	TLUSTY					CMFGEN					D [†]
			T_{eff} (10 ³ K)	log g (dex)	ξ (km s ⁻¹)	$v \sin i$ (km s ⁻¹)	D [†]	S/N ratio	T_{eff} (10 ³ K)	log g (dex)	ξ (km s ⁻¹)	$v \sin i$ (km s ⁻¹)	
152235	V900 Sco	B0.7Ia	22.7	2.70	15	76	1	400	23.0	2.65	10	81	3
154090	V1073 Sco	B0.7Ia	22.3	2.70	16	80	1	420	22.5	2.65	10	78	3
148688	V1058 Sco	B1Ia	20.6	2.50	16	71	1	435	22.0	2.60	15	72	3
14956	V475 Per	B1.5Ia ^a	19.4	2.40	20	75	2	370	21.0	2.50	10	80	2
14818	V554 Per	B2Ia ^a	18.8	2.40	18	76	2	240	18.5	2.40	20	82	2
14143		B2Ia ^a	19.1	2.40	18	72	2	230	18.0	2.25	20	76	2
53138	σ^2 CMa	B3Ia ^a	15.2	2.00	18	48	1	330	15.5	2.05	20	58	4

D[†]=Data source: 1 = FEROS, MPG/ESO 2.2-m telescope; 2 = ISIS, WHT; 3 = Loral 1 K spectrograph, CTIO; 4 = Richardson-Brealey spectrograph, JKT.

Table 2. Adopted atmospheric parameters for the sample stars (nine supergiants and two main-sequence stars). Spectral types are from the Bright Star Catalogue (Hoffleit & Warren 1995), with additional data from Perryman et al. (1997)^a, Schmidt & Carruthers (1995)^b and Lennon et al. (1992)^c. All of the objects have been observed using FEROS on the MPG/ESO 2.2-m telescope.

HD Number	Name	Spectral Type	T_{eff} (10 ³ K)	log g (dex)	ξ (km s ⁻¹)	$v \sin i$ (km s ⁻¹)	S/N ratio
155985		B0.5Iab ^a	23.4	3.00	13	63	370
108002		B1Iab ^a	20.4	2.70	16	65	385
142758	V361 Nor	B1.5Ia ^a	19.0	2.50	22	65	415
141318	V360 Nor	B2II	20.6	3.30	13	43	475
53138	σ^2 CMa	B3Ia ^c	15.2	2.00	18	48	330
51309	ι CMa	B3II	16.6	2.30	19	49	370
159110		B4Ib ^b	20.1	3.30	10	18	500
164353	67 Oph	B5II ^c	15.8	2.60	23	9	500
91619	V369 Car	B7Iae	13.2	1.80	20	29	500
126341	τ^1 Lup	B2IV	21.5	3.65	3	18	500
79447	ι Car	B3III	18.0	3.60	9	0	420

ionization balance with lines of Si II (4128 and 4130 Å), Si III (4552, 4568 and 4574 Å) and Si IV (4089 Å). The Si III and Si IV lines were used for B0.7 – B2 supergiants, and Si II/Si III for B2.5 – B3 objects.

The TLUSTY atmospheric parameters have been determined using an interrelated iterative process (see Thompson et al. 2006, 2007). Effective temperatures, T_{eff} , were determined using the silicon ionization balance from the multiplets of Si II (4128, 4130 Å) and Si III (4552, 4567, 4574 Å) and the Si IV line at 4116 Å (also the 4088 Å Si IV line for HD 126341). Similarly to Crowther et al. (2006), the Si III/Si IV lines were employed for stars in the spectral range B0.5–B1.5, while Si II/Si III lines were used for B2–B7 objects. However, Crowther et al. (2006) employed the Si IV line at 4088 Å (which can be blended with O II 4089.29 Å) rather than 4116 Å, as used here. In the B1.5 and B2 stars, in addition to other silicon lines, blended or weak features of both Si II and Si IV were observed and the use of these lines is discussed below.

Surface gravity estimates, log g , were obtained by overplotting theoretical profiles on to the observed spectra in the region of the Balmer lines, with an associated error of ± 0.2 dex due to the uncertainty in profile fitting. Note that

only the Balmer lines H δ and H γ have been used, as wind effects appear small for these lines but can be significant for H α and H β (McErlean et al. 1999). The microturbulence, ξ , was determined using the Si III multiplet around ~ 4560 Å, by plotting abundance against line strength and determining when the gradient is zero. O II lines were not used as microturbulence estimates from this species yields larger values than those from Si III lines, especially in the case of supergiants (McErlean et al. 1999; Trundle et al. 2004). Values of ξ in Tables 1 and 2 have uncertainties of at least 5 km s⁻¹.

The effect of rotational line broadening, $v \sin i$, was calculated by overlaying instrumentally broadened theoretical profiles, with the appropriate atmospheric parameters, on to the individual lines of the Si III multiplet. Theoretical profiles were scaled to the same equivalent width as the observed features, convolved to the same spectral resolution, and then rotationally broadened and overlain on to the spectra, to determine the most appropriate $v \sin i$ value (see Hunter et al. 2007 for further details). Other large-scale forms of broadening, such as macroturbulence (see for example Ryans et al. 2002), were not considered due to the difficulty in distinguishing between types of broadening through profile fitting. Thus, the derived $v \sin i$ values should be con-

sidered as upper limits. With the exception of HD 53138, these estimates agreed with those of Howarth et al. (1997) and Crowther et al. (2006) to within $\pm 6 \text{ km s}^{-1}$.

As stated above, in the B1.5 and B2 stars, blended or weak features were observed for Si II and Si IV. In the cases of HD 126341, HD 14956, HD 142758 and HD 141318, the Si II/Si III ionization balance gave a T_{eff} estimate approximately 900 K larger than obtained using the Si III/Si IV lines, with the gravity estimate changing by ~ 0.1 dex. As all of the features appear reliable, intermediate values of T_{eff} and $\log g$ were considered the most appropriate for the objects and these are listed in Tables 1 and 2. For the other B2 objects (HD 14818 and HD 14143), the Si II lines were used, as the Si IV features appeared weak and unreliable and thus were not employed to estimate the effective temperature.

The atmospheric parameters of HD 152235, HD 154090, HD 14956, HD 14818 and HD 14143 lie at or below the lowest available gravity point in the metal line grid. However, using the method detailed above, it was possible to deduce atmospheric parameters by extrapolating the silicon abundance estimates, and fitting the Balmer lines using the higher resolution grid. This was not believed to be a significant source of error, as tests performed using the available grid points indicated a difference of < 0.1 dex between silicon abundances determined using adjacent grid points.

In general, good agreement is found between the atmospheric parameters of the two studies, within the errors, despite the use of different model atmospheres. Comparing the temperature structures of CMFGEN and TLUSTY as a function of the Rosseland optical depth for HD 53138 (Fig. 1), indicates that the temperature structures are in good agreement in the regions of formation for Fe III and Si III, i.e. $\log_{10}(\text{Rosseland optical depth}) \sim -1.8$ and -1.5 , respectively. However, there are differences in the temperature and gravity estimates for HD 148688, HD 14956 and HD 14143. This may be due to the use of different silicon lines, especially as the CMFGEN and TLUSTY atmospheric parameters were deduced from the same observational data for the latter two objects. The $v \sin i$ values found here tend to be lower than those of Crowther et al. (2006), with the exception of HD 154090. In general, the $v \sin i$ estimates derived here are thought to be more reliable due to the improved observational data and methods of analysis.

3.3 Iron line selection and abundances

Fe III lines were identified from synthetic spectra produced with the TLUSTY line list, using a similar method to that discussed by Grigsby et al. (1996). Spectra were computed covering the wavelength range observed with the FEROS data, with atmospheric parameters corresponding to a typical B-type star of spectral type B2, e.g. HD 141318, as this spectral type appears to have the strongest Fe III spectrum from our sample. (Our models indicated that Fe III peaks at $T_{\text{eff}} \sim 21000 \text{ K}$). Two sets of abundances were considered; one with a solar abundance for all elements, and the other with all elements excluded apart from iron. These were then overplotted on to the HD 141318 spectra and examined for Fe III features. This process was then repeated for the B3 object HD 79447 to confirm the selection. This object was chosen despite having a weaker Fe III spectrum than the B2

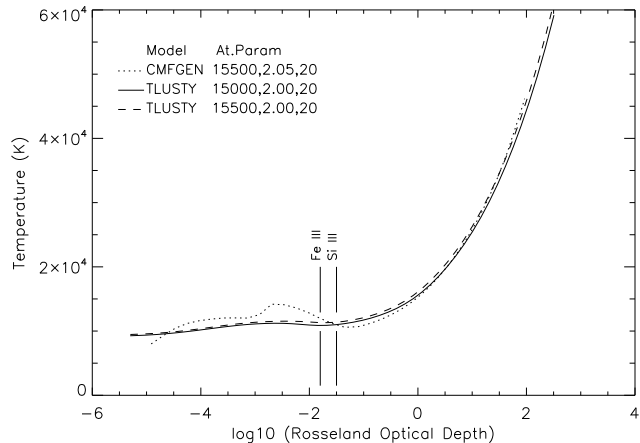


Figure 1. Temperature structure plotted against Rosseland mean optical depth for CMFGEN and TLUSTY, with the curves representing the different atmospheric parameters (At.param: T_{eff} , $\log g$ and ξ) for HD 53138, as calculated using the two models. The TLUSTY curves are for the closest available grid points to the derived parameters of $T_{\text{eff}} = 15200 \text{ K}$ and $\xi = 18 \text{ km s}^{-1}$. The regions of formation for Fe III and Si III are indicated.

objects, as it is a slower rotator and hence possible blended features could be more easily identified.

The amount of rotational line broadening in the theoretical spectra was increased to observe the effects on the identified lines. If two or more iron features could not be resolved, these were treated as blends within TLUSTY. Where an Fe III line was blended with an element of a different species, e.g. O II, the iron line was included provided that the features could be adequately resolved from each other. A number of Fe III lines that have been considered in previous studies were excluded from our investigation if they were deemed too weak or blended with other species. In particular, we note the following:

- The feature at 4395 \AA , detected by van Helden (1972a); Pintado & Adelman (1993) and Liu et al. (1998), was found to be blended with O II at 4395.93 \AA .
- A Fe III line at 4168.40 \AA , included by Pintado & Adelman (1993), is a blend of Fe III (4168.45 \AA) and S II (4168.38 \AA).
- For the Fe III lines around 4372 \AA it was not possible to resolve the individual features in the TLUSTY models, or in the slowest rotating object, HD 79447. Also, they appear to be blended with C II lines.
- There are a number of Fe III lines in the range $\sim 5880 - 6000 \text{ \AA}$, but this spectral region contains telluric transitions, making identification and measurement difficult.

As noted in Section 3.1, all of the TLUSTY (LTE) abundance estimates were generated using the Galactic grid and are given in Tables 4, 5 and 6. The CMFGEN (non-LTE) abundances (also shown in Table 4) were obtained by calculating synthetic spectra for each star, using the appropriate atmospheric parameters, for iron abundances of $\text{Fe} = 7.35, 7.65$ and 7.95 dex. Equivalent widths were then measured and compared to the observed values, and abundances obtained by interpolation or extrapolation. As for the TLUSTY models, this should normally not lead to significant errors. In Table

Table 3. Sample of the Fe III wavelengths and transitions, with atomic data taken from the Kurucz database^a (<http://nova.astro.umd.edu>, Hubeny 1988; Hubeny & Lanz 1995; Hubeny et al. 1998) and Nahar & Pradhan (1996)^b. Full details available on-line.

Wavelength (Å)	Transition ^b	g_i^b	g_j^b	Kurucz ^a log gf	N&P ^b log gf	Wavelength (Å)	Transition ^b	g_i^b	g_j^b	Kurucz ^a log gf	N&P ^b log gf
3953.76	$d^3G^e-w^3G^o$	9	9	-1.834	-2.153	4365.64	$a^5P^e-z^5P^o$	3	3	-3.404	-3.305
4005.04	$e^3F^e-z^3F^o$	9	9	-1.755	-1.810	4371.34	$a^5P^e-z^5P^o$	7	5	-2.992	-2.813
4022.11	$c^5F^e-t^5F^o$	9	9	-3.268	-3.438	4382.51	$a^5P^e-z^5P^o$	5	5	-3.018	-3.562
4022.35	$e^3F^e-z^3F^o$	7	7	-2.054	-1.967	4419.60	$a^5P^e-z^5P^o$	7	7	-1.690	-2.516
4035.43	$y^7P^o-c^7S^e$	5	7	0.119	0.147	4431.02	$a^5P^e-z^5P^o$	5	7	-2.572	-2.819
4039.16	$e^3F^e-z^3F^o$	5	5	-2.349	-2.091	4569.76	$d^1G^e-y^1G^o$	9	9	-1.870	-1.701
4053.11	$y^7P^o-c^7S^e$	7	7	0.261	0.291	5063.42	$b^5D^e-z^5P^o$	1	3	-2.950	-3.087
4053.47	$u^5F^o-g^5D^e$	3	5	-1.439	-1.273						

4, the absolute abundance estimates from the TLUSTY models, for HD 152235, HD 154090, HD 14956, HD 14818 and HD 14143, have been extrapolated, as the atmospheric parameters lie at or below the lowest available gravity grid points. However, tests using the available grid points indicate that this method yields reliable abundance estimates and should not lead to significant errors.

The abundance values have associated errors due to both systematic and random errors (see Hunter et al. 2005 for further details). For the TLUSTY comparisons, systematic errors arise due to the uncertainties in the atmospheric parameters, and are estimated by varying the parameters by their associated errors. These error estimates have also been adopted for the CMFGEN comparison. Random errors are related to the data analysis, such as the oscillator strengths, uncertainties in observations and line fitting errors. Thus, the random uncertainty is assumed to be the standard deviation of the abundance estimates from individual features, divided by the square root of the number of lines observed for that species. The total uncertainty is then taken as the square root of the sum of the squares of the systematic and random errors.

4 RESULTS AND DISCUSSION

4.1 Comparison of CMFGEN and TLUSTY results

As discussed in Section 3.1, there are different physical assumptions in the model atmosphere codes CMFGEN and TLUSTY. In particular, TLUSTY assumes plane-parallel geometry, while CMFGEN uses spherical geometry and considers wind properties. Additionally, non-LTE effects have been included in the CMFGEN Fe III calculations. The effects of the different assumptions on Fe III are considered for the sample of supergiants, shown in Table 1, which includes the atmospheric parameters determined here using TLUSTY and from Crowther et al. (2006). Table 4 shows the absolute abundance estimates deduced using the two model atmosphere codes, with the average values calculated from all of the observed Fe III features, with the exception of those at 4053 and 4222 Å. In the CMFGEN models with higher temperature and lower iron abundance, these features go into emission, and thus no abundance estimates could be obtained for the B0.7 – B1.5 objects. To maintain consistency, these lines

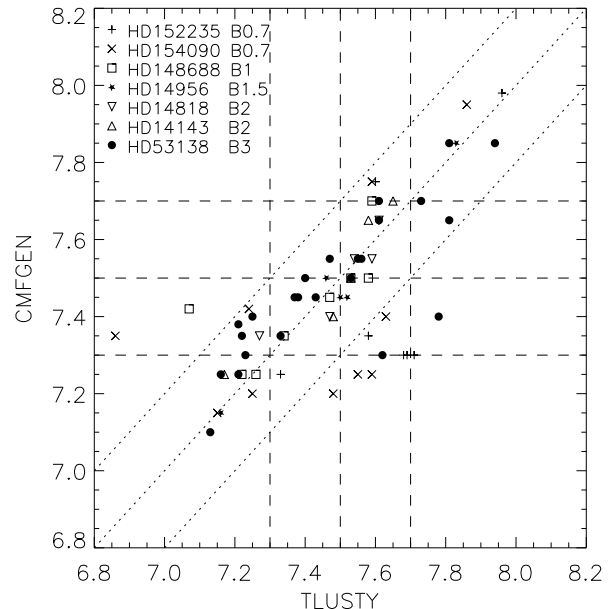


Figure 2. Abundance estimates from TLUSTY plotted against those from CMFGEN for Fe III features in all the comparison supergiants. The (· · ·) lines represent the $x = y$ (45°) relation (plus offsets of ± 0.2 dex), while the (---) lines represent $x = y \pm 0.5$ dex (plus ± 0.2 dex offsets).

have also been excluded in the B2 – B3 stars, but this does not significantly affect the average values.

In general, the average abundance estimates are in excellent agreement, having a typical difference of less than 0.05 dex, with HD 152235 displaying a larger discrepancy of 0.18 dex. Differences in the abundance estimates for the individual lines are generally less than 0.2 dex, although there are some exceptions. Fig. 2 shows the abundance estimates from TLUSTY and CMFGEN for each Fe III transition observed in all the supergiants. Assuming that all the stars have the same iron abundance, these values would be expected to be concentrated around a single point. To investigate possible sources of error two approaches have been adopted. Firstly, if errors due to the use of different physical assumptions predominate, abundance estimates would be transposed either

horizontally or vertically. Given the simplification adopted in the TLUSTY calculations, horizontal shifts would appear more probable. Alternatively, if errors were present in both analyses (for example, due to incorrect oscillator strengths), points would be shifted along a 45° line. To illustrate the former, horizontal and vertical loci at an abundance of 7.5 dex (typical of the Galactic value) plus offsets by ± 0.2 dex are illustrated, while for the latter, loci at 45° plus offsets by ± 0.2 dex are shown.

From Fig. 2, the majority of points appear to lie along the 45° line. However, there are some estimates which fall outside of this relation. These are due to the 5833 Å line (in HD 154090 and HD 148688), and most of the features in the spectral range 4419–5193 Å observed in the two B0.7 stars (HD 152235 and HD 154090). This suggests that the differences in physical assumptions may become more significant at higher temperatures and longer wavelengths. High abundance estimates situated along the 45° relation include the 4273 and 4296 Å features, which are from the same multiplet, suggesting that the oscillator strengths of this multiplet may be too low. Conversely, estimates due to the 4005 Å line for almost all of the supergiants are low, strongly suggesting that the adopted oscillator strength of this transition is too high. There are also other anomalous points, due to lines at 4164, 4166, 4352, 5193, 5306 and 5573 Å. These features, when observed in other objects, have abundance estimates situated between the horizontal loci, thus making it difficult to confirm their behaviour.

The Fe ionization structure included in the model atmosphere codes CMFGEN and TLUSTY may not be correct, potentially leading to erroneous estimates of the relative strengths of Fe II, Fe III and Fe IV lines. Examining the Fe ionization structure in CMFGEN, in cooler stars (e.g. HD 53138) Fe²⁺ is found to be dominant in the region of Fe III line formation. However, in the hotter stars (e.g. HD 152235) Fe²⁺ and Fe³⁺ compete for dominance in the Fe III line formation region. Incorrect ionization structure should lead to a similar shift observed along the 45° line for all the Fe III lines. However, such a trend is not observed in the sample of supergiants, suggesting that uncertainties in the ionization structure are not a significant source of error.

Therefore, the major sources of error appear to be present in both analyses, as the points are distributed along the 45° line. The most likely causes are observational uncertainties, such as equivalent width measurements, due to blending and poor quality data (especially in the later spectral type objects), or incorrect $\log gf$ values. Differences between the average abundances obtained from the two approaches are relatively minor, as there are few points lying outside the 45° relation. Thus, it appears that in general the different physical assumptions, in particular non-LTE effects, are small and a LTE approximation may be a reliable assumption for the Fe III spectrum in B-type stars.

4.2 Assessment of individual Fe III lines

Although the mean stellar abundance estimates agree, to within the errors, with the Galactic metallicity value, the reliability of the individual features varies. The majority of the Fe III features observed are due to single lines or blends of lines from the same multiplet, but some are blends with other multiplets (see Table 3). The reliability of individual

lines is discussed below in terms of equivalent width measurements and abundance estimates (see Tables 5 and 6).

- *3953 Å*: A weak feature only observed in the narrowest-lined stars (HD 159110, HD 126341 and HD 79447). Abundance estimates for this line are in excellent agreement with the average for these objects.

- *4005, 4022, 4039 Å*: The 4005 Å line is a relatively weak feature and is situated in the wings of He I 4009 Å. Its abundance estimate is consistently lower than the average for the individual objects by more than 0.15 dex. However, the other two features (4022 and 4039 Å) yield similar abundances, indicating that the values for this multiplet are consistent, although there may be problems with the oscillator strengths. The 4022 Å feature in the supergiant HD 159110 gives a larger abundance than the other features observed, by ~ 0.4 dex, suggesting it may not be reliable.

- *4035, 4053, 4081 Å*: The 4035 Å line observed in HD 79447 yields a larger abundance than the other features of this multiplet. This may be due to blending with N II 4035.10 Å and O II 4035.49 Å, making the equivalent width measurement unreliable. The 4053 and 4081 Å features are in good agreement, despite 4053 Å being a blend of two lines. In general, their abundance estimates are lower than the average value obtained, and thus may not be reliable.

- *4122 – 4166 Å*: The 4164.92 Å feature is close to S II 4165.10 Å. However, this does not appear to be a problem, as the abundance estimate from the line agrees with that from other features in the same multiplet. The 4166 Å line in HD 51309 provides a low abundance as it is a weak feature. All lines apart from 4154 Å are blends but as the abundance values are consistent, this is not considered a significant source of error.

- *4222 – 4261 Å*: The 4222 Å feature consistently gives a larger abundance than the average for a given star, which may be due to this line being treated as a blend within TLUSTY and the difficulties in accurately determining the equivalent width, potentially leading to an overestimation of its value. Other features from the same multiplet are observed in HD 159110, HD 126341 and HD 79447. In the former two stars, the abundance estimates from these lines tend to be lower than that of 4222 Å, but in HD 79447 the 4248 Å line is in agreement with 4222 Å, suggesting the value may be reliable. The 4248 and 4261 Å lines are consistent for HD 79447 but not HD 159110. However the lines are extremely weak in the supergiant and hence have large uncertainties in their equivalent width measurements.

- *4273 – 4310 Å*: These features are all components of the same multiplet. In general they tend to give abundance estimates higher than the overall average for the stars in which they are observed. In the two main-sequence stars, these lines agree well, while in the supergiants 4273 Å tends to yield a larger value than both the average abundance estimate and those from the other lines of the multiplet. This may be due to the line being close to O II 4273.10 Å, and thus it is difficult to resolve in stars with broader features.

Table 4. Fe III equivalent width measurements (EW)* and absolute abundance estimates[◊] for the supergiants derived using TLUSTY (T; LTE) and CMFGEN (C; non-LTE).

Wavelength (Å)	HD 152235			HD 154090			HD 148688			HD 14956			HD 14818			HD 14143			HD 53138		
	EW (mÅ)	T [†]	C	EW (mÅ)	T [†]	C	EW (mÅ)	T	C	EW (mÅ)	T [†]	C	EW (mÅ)	T [†]	C	EW (mÅ)	T [†]	C	EW (mÅ)	T	C
4005.04	17 c	7.33	7.25	14 c	7.15	7.15	24 c	7.22	7.25	28 c	7.16	7.15	37 c	7.27	7.35	30 c	7.17	7.25	25 b	7.23	7.30
4053.00 ^a	20 c	7.56	×	7 c	7.24	7.35
4164.00 ^a	23 c	7.22	7.35
4166.00 ^a	8 c	7.21	7.25
4222.00 ^a	17 c	7.67	×	19 c	7.64	×	23 c	7.75	×	19 c	7.56	×	24 b	7.70	7.95	26 c	7.74	7.81	18 b	7.97	8.15
4273.00 ^a	16 c	7.96	7.98	16 c	7.86	7.95	16 c	7.83	7.85	10 c	7.61	7.65	11 c	7.65	7.77	8 c	7.94	7.85
4296.00 ^a	14 c	7.60	7.75	16 c	7.59	7.75	15 c	7.59	7.70	16 c	7.58	7.65	10 c	7.81	7.65
4310.00 ^a	11 c	7.24	7.42	17 c	7.46	7.50	19 c	7.54	7.55	9 c	7.56	7.55
4352.58	23 c	7.13	7.10
4382.51	21 c	7.81	7.85
4419.60	50 c	7.58	7.35	45 c	7.55	7.25	70 c	7.58	7.50	91 b	7.52	7.45	87 b	7.47	7.40	87 b	7.48	7.40	86 a	7.55	7.55
4431.02	51 c	7.50	7.45	66 c	7.59	7.55	56 c	7.53	7.50	59 b	7.61	7.65
5063.42	16 c	7.38	7.45
5086.00 ^a	25 c	7.63	7.40	29 c	7.53	7.50	41 b	7.61	7.70
5127.00 ^a	69 a	7.71	7.30	59 c	7.48	7.20	60 c	7.26	7.25	93 a	7.47	7.55
5156.11	70 b	7.69	7.30	77 b	7.59	7.25	73 c	7.34	7.35	90 a	7.40	7.50
5193.91	26 c	7.68	7.30	16 c	7.25	7.20	26 c	7.21	7.38
5235.66	26 c	7.78	7.40
5272.00 ^a	9 c	7.33	7.35
5276.00 ^a	23 c	7.62	7.30
5282.00 ^a	18 c	7.37	7.45
5299.93	12 c	7.43	7.45
5302.60	15 c	7.53	7.50
5306.00 ^a	50 c	7.25	7.40
5573.42	24 c	7.47	7.45	8 c	7.16	7.25
5833.94	29 c	6.86	7.35	46 b	7.07	7.42	50 a	7.73	7.70
Average [‡]		7.65	7.46		7.42	7.39		7.38	7.43		7.49	7.48		7.50	7.50		7.48	7.50		7.46	7.47
±		0.42	0.44		0.36	0.36		0.18	0.18		0.13	0.18		0.06	0.09		0.08	0.09		0.18	0.18

* Equivalent width measurements: ‘a’: accurate to better than ± 10 per cent, ‘b’: to better than ± 20 per cent, and ‘c’: to less than ± 20 per cent.

† Extrapolation of values due to atmospheric parameters being on/below the available TLUSTY grid point.

◊ Logarithmic abundance $[M/H]$ on the scale $\log[H] = 12.00$ (dex).

^a Treated as blends in TLUSTY.

‡ Calculated using all lines except those at 4053 and 4222 Å.

× No abundance estimate due to CMFGEN model appearing to go into emission.

Table 5. Fe III absolute abundance estimates (Ab. $^{\diamond}$) and equivalent width measurements (EW)* for the supergiants.

Wavelength (Å)	HD 155985		HD 108002		HD 142758		HD 141318		HD 51309		HD 53138		HD 159110		HD 164353		HD 91619	
	EW (mÅ)	Ab.	EW (mÅ)	Ab.	EW (mÅ)	Ab.	EW (mÅ)	Ab.	EW (mÅ)	Ab.	EW (mÅ)	Ab.	EW (mÅ)	Ab.	EW (mÅ)	Ab.	EW (mÅ)	Ab.
3953.76	3 c	7.42
4005.04	28 c	7.18	47 b	7.39	26 c	7.25	24 c	7.13	25 c	7.23	18 b	7.14	13 c	7.05	12 c	7.16
4022.00 ^a	10 c	7.60
4039.16	10 c	7.21	9 c	7.15
4053.00 ^a	17 c	7.41	7 c	7.24	13 b	7.28
4081.01	13 c	7.21
4122.00 ^a	30 c	7.27
4137.00 ^a	24 c	7.21
4139.00 ^a	24 c	7.19
4154.96	8 c	7.40
4164.00 ^a	53 b	7.23	62 b	7.49	28 c	7.13	23 c	7.22	42 c	7.29	21 c	7.21	14 c	7.42
4166.00 ^a	24 c	7.36	29 b	7.56	5 c	6.84	8 c	7.21	16 c	7.29	6 c	7.23	5 c	7.33
4222.00 ^a	20 c	7.60	23 c	7.64	56 b	8.13	32 a	7.93	20 b	7.83	18 b	7.97	23 a	7.81	10 c	7.71	10 b	8.11
4238.62	7 c	7.34
4248.00 ^a	5 c	7.35
4261.00 ^a	4 c	7.56
4273.00 ^a	17 c	7.82	20 c	7.91	24 c	8.02	18 c	7.95	8 c	7.94	11 c	7.75	6 c	7.89
4286.00 ^a	12 c	7.65
4296.00 ^a	16 c	7.53	21 c	7.64	34 c	7.95	17 c	7.66	11 c	7.59	10 c	7.81	11 c	7.52	14 c	7.97
4304.00 ^a	14 c	7.55	5 c	7.47
4310.00 ^a	18 c	7.43	23 c	7.55	39 c	7.88	30 c	7.78	11 c	7.47	9 c	7.56	16 b	7.56	5 c	7.36
4352.58	23 c	7.13	15 c	7.14	20 c	7.26
4365.64	7 c	7.22
4371.34	18 c	7.18
4382.51	16 c	7.84	21 c	7.81	13 c	7.78	11 c	7.67	11 c	7.69
4419.60	41 c	7.51	81 b	7.52	129 a	7.68	63 a	7.51	81 a	7.44	86 a	7.55	42 a	7.32	51 a	7.38	55 b	7.48
4431.02	37 c	7.79	52 c	7.56	89 c	7.76	43 c	7.58	55 b	7.53	59 b	7.61	27 b	7.40	36 c	7.52	41 c	7.62
5063.42	32 c	7.64	12 c	7.39	19 b	7.42	16 c	7.38	11 c	7.39	11 c	7.45	13 c	7.50
5086.00 ^a	19 c	7.53	41 b	7.58	65 c	7.75	34 c	7.65	37 b	7.53	41 b	7.61	21 c	7.47	25 b	7.58	27 c	7.67
5127.00 ^a	53 b	7.45	102 a	7.46	139 a	7.57	79 a	7.50	93 a	7.40	93 a	7.47	53 a	7.31	54 b	7.35	65 b	7.49
5156.11	62 b	7.49	111 a	7.49	145 a	7.55	74 a	7.41	93 a	7.34	90 a	7.40	43 a	7.17	46 b	7.21	56 b	7.35
5193.91	29 c	7.22	43 c	7.36	29 c	7.42	31 b	7.25	26 c	7.21	20 b	7.27	21 c	7.35	21 c	7.35
5235.66	27 c	7.42	18 c	7.35	32 c	7.68	30 c	7.69	26 c	7.78	18 b	7.45
5272.00 ^a	38 c	7.55	26 c	7.56	11 c	7.21	10 c	7.33	18 b	7.43	12 c	7.64
5276.00 ^a	36 c	7.40	31 b	7.57	19 c	7.35	23 c	7.62	21 b	7.41	27 c	7.94
5282.00 ^a	36 c	7.28	42 b	7.64	20 c	7.27	18 c	7.37	25 a	7.41	9 c	7.26	7 c	7.35
5284.00 ^a	11 c	7.37	14 c	7.60	7 c	7.36
5299.93	23 c	7.56	19 c	7.50	12 c	7.29	12 c	7.43	13 c	7.31
5302.60	24 c	7.53	22 c	7.52	12 c	7.25	15 c	7.53	14 c	7.33
5306.00 ^a	15 c	7.55	21 c	7.67	9 c	7.31	6 c	7.25	11 c	7.43
5573.42	32 b	7.53	10 c	7.20	8 c	7.10	8 c	7.16	8 c	7.17
5833.94	48 b	7.14	73 a	7.33	134 a	7.77	80 a	7.80	56 a	7.59	50 a	7.73	46 a	7.52	26 b	7.57	24 a	7.99
6032.00 ^a	12 c	6.90	13 c	7.01
6036.00 ^a	12 c	7.73	6 c	7.48
Average		7.52		7.51		7.59		7.56		7.36		7.48		7.38		7.47		7.52
±		0.23		0.11		0.08		0.15		0.18		0.17		0.16		0.23		0.28

* Equivalent width measurements: ‘a’: accurate to better than ± 10 per cent, ‘b’: to better than ± 20 per cent, and ‘c’: to less than ± 20 per cent. $^{\diamond}$ Logarithmic abundance [M/H] on the scale $\log[H] = 12.00$ (dex).^a Treated as blends in TLUSTY.

• *4352 – 4431 Å*: None of the lines is a blend. The lines at 4419 and 4431 Å show good agreement for all stars, although in HD 155985 the 4431 Å abundance is slightly higher, due to the difficulty in resolving this feature in the spectra from N II 4431.81 Å. The 4352 Å line tends to give a lower abundance than the average, while 4382 Å gives a higher value. However, the overall abundance value for this multiplet appears reliable. The 4371 Å line is only reliably resolved in the main-sequence objects and HD 159110 as it is close to a strong blended feature at 4372 Å due to Fe III and C II. Another component of this multiplet, at 4395.76 Å, has been excluded as it is blended with O II 4395.93 Å (see Section 3.3).

• *4569 Å*: This feature is only observed in HD 79447 as it is intrinsically weak. The abundance obtained is lower than the average, and does not appear reliable.

• *5063 – 5193 Å*: These are strong, well identified features. The abundance estimates from these lines tend to vary around the average and appear reliable. The 5086 Å line is a blend of several transitions and gives a slightly larger abundance than the other lines (which are components of the same multiplet) for the supergiants, possibly due to poor S/N around the line. As this trend is not observed in the main-sequence stars, the line appears reliable.

• *5235 – 5282, 5299, 5302 Å*: For the main-sequence stars there is good agreement between the abundance estimates, but the line at 5299 Å yields a higher value for HD 79447, and 5276 Å for HD 164353. The 5276 Å feature is close to Fe II 5276.00 Å, which appears to affect the abundance estimates obtained for HD 164353. The Fe III line at 5235 Å is adjacent to Fe II 5234.62 Å. However, these lines are well resolved in all stars apart from the supergiants of spectral type B3. Thus for these objects (HD 51309 and HD 53138) the abundances may be higher due to the difficulty in measuring the individual equivalent widths. The blending of different transitions in the lines does not appear to affect the abundance estimates obtained.

• *5272, 5284, 5306 Å*: The 5272 and 5306 Å features contain transitions from several multiplets, whereas 5284 Å is a blend lines from the same multiplet. Good agreement is found among all the lines, although the 5284 Å abundance is slightly lower for HD 126341 and HD 142758, while the 5272 Å value is slightly lower in HD 79447. This is probably due to the lines being weak in these stars, but overall these lines appear reliable.

• *5375 Å*: This is a blend of two transitions, and is only observed in HD 126341. It has a small equivalent width and it gives a slightly lower than average abundance estimate.

• *5460 – 5573 Å*: The 5573 Å line tends to give a lower than average abundance. The abundances from the other lines are also slightly below the average, but are only observed in the main-sequence stars. In general these are weak lines and thus may not be reliable.

• *5833 Å*: The abundance from this feature varies around the average in the stars, despite being a strong, isolated, single transition, and this may be due to non-LTE effects.

• *5999 Å*: This line is situated close to telluric features (see Section 3.3) and is only resolved in HD 79447. However, this abundance estimate appears reliable as it agrees with the overall value for the star.

• *6032, 6036 Å*: The 6032 Å line gives a consistently lower than average abundance, while the 6036 Å abundance esti-

Table 6. Fe III equivalent width measurements (EW)* and absolute abundance estimates for the main-sequence stars.

Wavelength (Å)	HD 126341		HD 79447	
	EW (mÅ)	Abundance [◊]	EW (mÅ)	Abundance [◊]
3953.76	4 c	7.59	3 c	7.68
4005.04	17 b	7.38	14 c	7.39
4022.00 ^a	11 c	7.39	9 c	7.44
4035.43	6 c	7.90
4039.16	6 b	7.50
4053.00 ^a	12 b	7.43	6 b	7.45
4081.01	14 b	7.51	6 b	7.38
4122.03 ^{ab}	18 b	7.55	11 c	7.73
4122.78 ^{ab}	15 b	...	12 c	...
4137.00 ^a	28 b	7.61	12 b	7.39
4139.00 ^a	29 b	7.59	13 b	7.49
4154.96	7 c	7.47
4164.73 ^{ab}	41 c	7.70	15 c	7.50
4164.92 ^{ab}	7 c	...
4166.00 ^a	15 a	7.53	8 c	7.47
4222.00 ^a	23 a	8.14	8 a	7.80
4238.62	6 b	7.43	3 c	7.56
4248.00 ^a	8 c	7.56	7 c	8.02
4261.00 ^a	4 c	7.57	3 c	7.88
4273.00 ^a	8 c	7.64	5 b	7.94
4286.00 ^a	11 b	7.73	6 c	7.85
4296.00 ^a	13 a	7.78	7 b	7.90
4304.00 ^a	16 b	7.87	7 b	7.81
4310.00 ^a	17 b	7.88	8 b	7.80
4352.58	10 b	7.17	10 c	7.38
4365.64	5 c	7.24	7 c	7.55
4371.34	20 c	7.55	12 c	7.33
4382.51	11 c	7.93	11 b	8.02
4419.60	36 a	7.77	33 a	7.59
4431.02	24 b	7.68	23 a	7.68
4569.76	3 c	7.48
5063.42	11 b	7.58	10 c	7.71
5086.00 ^a	20 b	7.70	14 c	7.66
5127.00 ^a	52 a	7.67	55 b	7.77
5156.11	40 a	7.77	32 a	7.46
5193.91	19 b	7.49	14 c	7.55
5235.66	15 b	7.60	5 b	7.49
5272.00 ^a	9 b	7.52	6 b	7.58
5276.00 ^a	18 b	7.63	6 b	7.45
5282.00 ^a	20 a	7.60	10 b	7.59
5284.00 ^a	6 c	7.37	5 c	7.95
5299.93	13 b	7.51	9 b	7.83
5302.60	15 b	7.62	6 c	7.59
5306.00 ^a	11 c	7.58	8 c	7.91
5375.00 ^a	4 c	7.49
5460.80	9 c	7.52
5485.52	8 c	7.35	5 c	7.54
5573.42	9 b	7.28	2 c	7.16
5833.94	36 a	7.89	15 a	7.59
5999.00 ^a	10 c	7.69
6032.00 ^a	12 b	7.16	6 c	7.35
6036.00 ^a	5 c	7.38	2 c	7.71
Average		7.57		7.63
±		0.22		0.26

* EW measurements: ‘a’: accurate to better than ± 10 per cent, ‘b’: to better than ± 20 per cent, and ‘c’: to less than ± 20 per cent. [◊] Logarithmic abundance $[M/H]$ on the scale $\log[H] = 12.00$ (dex). ^a Treated as blends in TLUSTY. ^b Equivalent widths of adjacent lines were combined to produce the corresponding abundances shown.

Table 7. Summary of previously determined iron abundances from Reitermann et al. (1990) (R90), Niemczura & Daszyńska-Daszkiewicz (2005) (N05), Gies & Lambert (1992) (G92) and Proffitt & Quigley (2001) (P01).

HD Number	Abundance (dex)		$\Delta[\text{Fe}/\text{H}]$	Ref.
	This work	Previous Work		
79447	7.63	7.62 ^a	+0.01	R90
		7.66 ^b	-0.03	R90
126341	7.57	7.11 ^c	+0.46	N05
51309	7.36	7.51 ^c	-0.15	G92
		7.69 ^d	-0.33	G92
		6.93 ^e	+0.43	P01

^a Using Fe III lines, ^b Using Fe II lines, ^c $T_{\text{eff}} = 17390$ K, ^d $T_{\text{eff}} = 14860$ K, ^e Assuming a Galactic abundance of 7.50 dex,

mates have a larger scatter. These lines have relatively small equivalent widths, and do not appear reliable due to the low S/N of the region.

As there are a number of Fe III lines observed it is possible to compare microturbulence values obtained using the Fe III and Si III lines. In general, the values obtained are consistent, when using all of the Fe III features observed. The multiplets of a $^5\text{P}^e - ^5\text{P}^o$ (4352 – 4431 Å) and b $^5\text{D}^e - ^5\text{P}^o$ (5063 – 5193 Å) could be considered independently and are in good agreement with the overall result, provided well-observed lines are employed.

4.3 Comparison with previous studies

Most of our targets have been analysed previously. For HD 108002 and HD 159110, no previous results were found, while for HD 155985 and HD 142758 only projected rotational velocities have been determined (Balona 1975; Howarth et al. 1997). Only three of the objects have previous iron abundance estimates, namely HD 79447, HD 126341 and HD 51309. These are discussed below and summarized in Table 7.

Reitermann et al. (1990) analysed optical data taken with the CASPEC spectrograph on the 3.6-m telescope (ESO) for HD 79447, covering the 3900 – 4900 Å wavelength range. They obtained LTE atmospheric parameters of $T_{\text{eff}} = 17800$ K and $\log g = 3.50$ dex, and Fe II and Fe III iron abundances. Their Fe III (and overall iron) abundance is in excellent agreement with that found here.

In the case of HD 126341, *IUE* spectra spanning 1100 – 3200 Å were analysed with a best-fit procedure by Niemczura & Daszyńska-Daszkiewicz (2005). A metallicity was obtained, which is significantly lower than our value, possibly due to the use of UV spectra, as our atmospheric parameters agree well with theirs ($T_{\text{eff}} \sim 22700$ K and $\log g = 3.74$ dex).

There are two previous estimates for the iron abundance in HD 51309. Gies & Lambert (1992) analysed optical data from the McDonald 2.1-m telescope and coude spectrograph, identifying two Fe II and two Fe III lines. For the Fe III lines, we found a similar equivalent width to their value for 5063

Å, but for the 5156 Å feature their result is approximately 50 per cent of that measured here (54 mÅ compared to 93 mÅ). Also, they do not observe the line at 5193 Å, which we have detected, possibly due to the use of higher S/N spectra in the present paper. This was tested by degrading theoretical spectra, calculated using the appropriate atmospheric parameters (from Gies & Lambert 1992) and Fe abundance for the line (taken from this work), indicating that the feature may have been unclear due to noise. Gies & Lambert considered two different temperature estimates (17390 and 14860 K) and associated abundances. They state that their data are insufficient to distinguish between these temperatures. However, both temperature estimates are consistent with that found here (16600 K). Proffitt & Quigley (2001) also investigated HD 51309, using *IUE* SWP spectra to obtain an LTE abundance. Their value is much lower than the abundance derived by Gies & Lambert (1992) or that found here. As for HD 126341, this difference is believed to be due to the use of UV spectra rather than optical data, as their effective temperature (16570 K) and surface gravity (2.60 dex) agree well with our estimates.

It is worth noting that a selection of iron features have been considered in other studies, but with no abundances determined. Lennon et al. (1993) observed five of our sample of supergiants (HD 14956, HD 14818, HD 14143, HD 53138 and HD 164353). They note that several lines due to Fe III are visible (over the range 3950 – 4950 Å), but that they are relatively weak and hence unreliable. Van Helden (1972a,b) investigated HD 53138 and observed seventeen absorption features due to Fe III in their optical (3500 – 8800 Å) spectrograms, stating that fourteen are blended with lines of other spectra and giving equivalent width measurements for thirteen. While a number of these lines have been included here, several were excluded as they were considered unreliable due to blending with other features. For example, Fe III 4041.86 Å appears to be blended with O II 4041.95 Å (see Section 3.3). For the lines included here, the equivalent width measurements by van Helden (1972a) tend to be larger. Those listed here are believed to be more reliable due to the improved quality of the spectra.

5 CONCLUSIONS

Due to their intrinsic weakness, Fe III absorption lines have not been widely considered for use in chemical composition studies. Instead, the very rich ultraviolet spectral region has been favored. However, the results found in this paper suggest that the optical region can provide consistent results. The stars here display abundance estimates that agree with the Galactic metallicity, and are consistent with previous studies using optical spectra, where available. By contrast, previous determinations from ultraviolet spectra have followed the trends observed in other studies (for example Thompson et al. 2007; Dufton et al. 2007), providing lower abundance estimates, in these cases by approximately 0.5 dex.

Although our study has concentrated on B-type stars found in the Milky Way, the optical Fe III lines examined here can be applied to studies of B-type stars in other galaxies, provided suitable S/N spectra are employed. For example, Trundle et al. (2002) analysed a sample of B-type su-

Table 8. Recommended Fe III lines for use as abundance diagnostics.

Line (Å)	Spectral Type Range	Line (Å)	Spectral Type Range
4419	B0.5–B7	5156	B0.5–B7
4431	B1–B7	5272	B1.5–B5
5063	B1.5–B7	5282	B2–B7
5086	B0.5–B7	5299	B1.5–B4
5127	B0.5–B7	5302	B1.5–B4

pergiants in M31, obtaining an Fe abundance from the Fe III line at 4419 Å. Rolleston et al. (2002) analysed a sample of OB-type main-sequence stars from the LMC, finding an Fe abundance for one object (PS 34-16), while Rolleston et al. (2003) investigated a B-type dwarf from the SMC (AV 304), finding agreement with other giant stars. More recently, Trundle et al. (2007) used similar methods to those detailed here and obtained Fe abundances for B-type stars in the Galaxy, LMC and SMC, using the two Fe III lines at 4419 and 4430 Å. The results found were consistent with the present accepted metallicities of these systems. These studies indicate that the optical Fe III lines can provide reliable abundance indicators in different galaxies.

Our comparison of stars analysed using the model atmosphere codes CMFGEN and TLUSTY generally shows little difference in the abundance estimates, indicating that the different physical assumptions, in particular non-LTE effects, are small for this species. Therefore, the results suggest that the optical Fe III absorption line spectrum may be used with confidence in chemical composition studies, and an LTE analysis provides reliable results.

The atomic data of Nahar & Pradhan (1996), employed both in this paper and by Crowther et al. (2006), appear to provide appropriate abundances, although there are some features, such as those at 4005 and 4273 Å, whose $\log gf$ values may be incorrect. Comparing the values in Table 3 shows that, for some features, e.g. the 4166.88, 4419.60 and 5272.90 Å lines, there are large differences between the atomic data from the Kurucz database and Nahar & Pradhan (1996). Further work is required to refine the atomic data for this species.

In Table 8 we list recommended Fe III lines which we believe, based on the present study, will provide reliable diagnostics for the iron abundance in early B-type stars. Lines have been selected based on the following criteria:

- Relatively strong, isolated feature, free from known blends.
- Yields an abundance estimate within ± 0.2 dex of the mean iron abundance for all well observed lines.

The range of spectral types over which it is advisable to use the lines as an abundance diagnostic is also listed in Table 8. This spectral type range is not the same for all lines, generally due to the fact that some of the weaker transitions are only detected over a restricted span of spectral types. Observations for all of the lines in this Table are shown in Fig. 3 for HD 79447. The line at 5193 Å has been included in the Figure, but not the Table, because its derived abundance is more than 0.2 dex larger than the mean value for three of the stars studied here, namely HD 108002 (B1), HD 142768

(B1.5) and HD 53138 (B3). However, the feature, along with others observed (see Tables 4, 5 and 6) may be suitable for diagnostic use, depending on the quality of the spectra used. We note that the stars included in this study have been selected due to being narrow lined and are typical of their individual luminosity classes. However, if objects with larger $v \sin i$ values were employed, blending between Fe lines and other metal features may occur, thus, care should be taken when using objects with larger projected rotational velocities.

ACKNOWLEDGMENTS

HMAT acknowledges financial support from the Northern Ireland Department for Education and Learning (DEL). FPK is grateful to AWE Aldermaston for the award of a William Penney Fellowship.

REFERENCES

- Balona L. A., 1975, *MmRAS*, 78, 51
 Crowther P. A., Lennon D. J., Walborn N. R., 2006, *A&A*, 446, 279
 Cunha K., Lambert D. L., 1994, *ApJ*, 426, 170
 Dixon W. V., Hurwitz M., 1998, *ApJ*, 500, L29
 Dufton P. L., 1998, in *Boulder–Munich II*, Howarth I. D., eds, *ASP Conf. Ser. Vol. 131.*, Properties of Hot, Luminous Stars. Astron. Soc. Pac., San Francisco, p. 169
 Dufton P. L., Brown P. J. F., Fitzsimmons A., Lennon D. J., 1990, *A&A*, 232, 431
 Dufton P. L., Ryans R. S. I., Trundle C., Lennon D. J., Hubeny I., Lanz T., Allende Prieto C., 2005, *A&A*, 434, 1125
 Dufton P. L., Ryans R. S. I., Thompson H. M. A., Street R. A., 2007, *MNRAS*, submitted
 Esteban C., Peimbert M., Torres-Peimbert S., Rodriguez M., 2002, *ApJ*, 581, 241
 Evans C. J., Crowther P. A., Fullerton A. W., Hillier D. J., 2004, *ApJ*, 610, 1021
 Gies D. R., Lambert D. L., 1992, *ApJ*, 387, 673
 Gilmore G., Wyse R. F. G., 1998, *AJ*, 116, 748
 Grevesse N., Sauval A. J., 1998, *Space Sci. Rev.*, 85, 161
 Grigsby J. A., Mulliss C. L., Baer G. M., 1996, *PASP*, 108, 953
 Hardorp J., Scholz M., 1970, *ApJS*, 19, 193
 Hatzidimitriou D., Reig P., Manousakis A., Pietsch W., Burwitz V., Papamastorakis I., 2007, *A&A*, 464, 1075
 Heber U., 1983, *A&A*, 118, 39
 Hillier D. J., Lanz T., 2001, in *Ferland G., Wolf Savin D.*, eds, *ASP Conf. Ser. Vol. 247.*, Spectroscopic Challenges of Photoionized Plasmas. Astron. Soc. Pac., San Francisco, p. 343
 Hillier D. J., Miller D. L., 1998, *ApJ*, 496, 407
 Hillier D. J., Lanz T., Heap S. R., Hubeny I., Smith L. J., Evans C. J., Lennon D. J., Bouret J. C., 2003, *ApJ*, 588, 1039
 Hoffleit D., Warren W. H. Jr., 1995, *Bright Star Catalogue*, 5th Revised Ed. (Hoffleit+, 1991). *VizieR On-line Data Catalog: V/50*

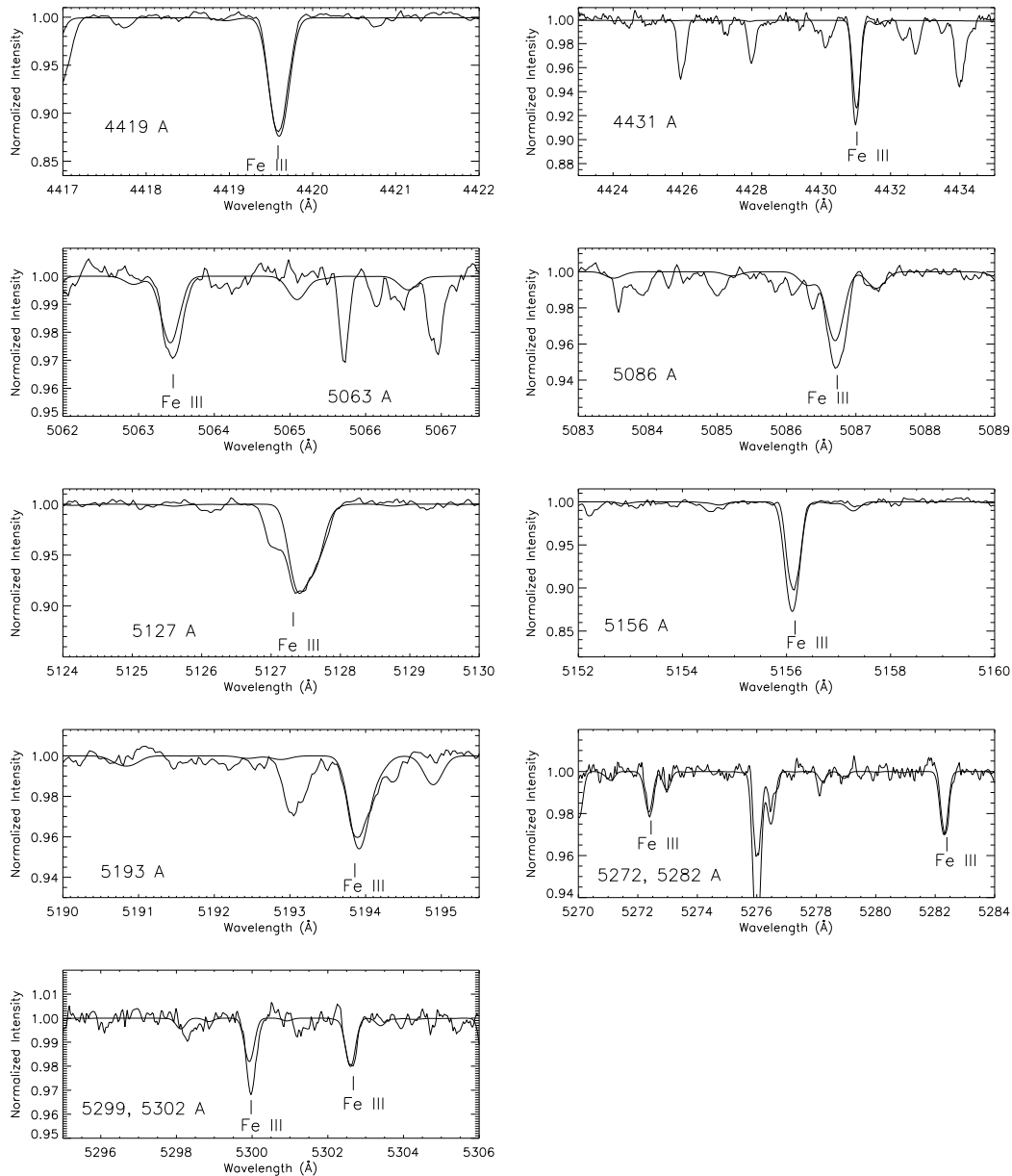


Figure 3. Observed Fe III lines in HD 79447 as listed in Table 8, including the 5193 Å line. Overplotted are theoretical fits (smooth line) to the Fe III lines, calculated using the average abundance estimate for the star of 7.63 dex.

Howarth I. D., Siebert K. W., Hussain G. A. J., Prinja R. K., 1997, MNRAS, 284, 265

Howarth I. D., Murray J., Mills D., Berry D. S., 2004, Starlink User Note 50.24: DIPSO – A Friendly Spectrum Analysis Program, Rutherford Appleton Laboratory/CCLRC, Didcot

Hubeny I., 1988, Comput. Phys. Commun., 52, 103

Hubeny I., Lanz T., 1995, ApJ, 439, 875

Hubeny, I., Heap, S.R., Lanz, T., 1998, in Boulder–Munich II, Howarth I. D., eds, ASP Conf. Ser. Vol. 131., Properties of Hot, Luminous Stars. Astron. Soc. Pac., San Francisco, p. 108

Hummer D. G., Berrington K. A., Eissner W., Pradhan A. K., Saraph H. E., Tully J. A., 1993, A&A, 279, 298

Hunter I., Dufton P. L., Ryans R. S. I., Lennon D. J., Rolleston W. R. J., Hubeny I., Lanz T., 2005, A&A, 436, 687

Hunter I., Dufton P. L., Smartt S. J., Ryans R. S. I., Evans C. J., Lennon D. J., Trundle C., Hubeny I., Lanz T., 2007, A&A, 466, 277

Kaufer A., Stahl O., Tubbesing S., Norregaard P., Avila G., Francois P., Pasquini L., Pizzella A., 1999, The Messenger, 95, 8

Kendall T. R., Conlon E. S., Dufton P. L., Keenan F. P., 1994a, A&A, 290, 563

Kendall T. R., Brown P. J. F., Conlon E. S., Dufton P. L., Keenan F. P., 1994b, A&A, 291, 851

Kilian J., 1992, A&A, 262, 171

Kilian J., 1994, A&A, 282, 867

- Korn A. J., Becker S. R., Gummersbach C. A., Wolf B., 2000, *A&A*, 353, 655
- Lennon D. J., Dufton P. L., Fitzsimmons A., 1992, *A&AS*, 94, 569
- Lennon D. J., Dufton P. L., Fitzsimmons A., 1993, *A&AS*, 97, 559
- Liu Z., Sterken C., Zhao F., 1998, *JAD*, 4, 1
- McErlean N. D., Lennon D. J., Dufton P. L., 1999, *A&A*, 349, 553
- McKenna F. C., Keenan F. P., Hambly N. C., Allende Prieto C., Rolleston W. R. J., Aller L. H., Feibelman W. A., 1997, *ApJS*, 109, 225
- Moehler S., Heber U., Lemke M., Napiwotzki R., 1998, *A&A*, 339, 537
- Mokiem M. R., et al., 2007, *A&A*, 465, 1003
- Mooney C. J., Rolleston W. R. J., Keenan F. P., Dufton P. L., Smoker J. V., Ryans R. S. I., Aller L. H., Trundle C., 2004, *A&A*, 419, 1123
- Morel T., Butler K., Aerts C., Neiner C., Briquet M., 2006, *A&A*, 457, 651
- Nahar S. N., Pradhan A. K., 1996, *A&AS*, 119, 509
- Napiwotzki R., Heber U., Köppen J., 1994, *A&A*, 292, 239
- Niemczura E., Daszyńska-Daszkiewicz J., 2005, *A&A*, 433, 659
- Peters G. J., 1976, *ApJS*, 30, 551
- Peters G. J., Aller L. H., 1970, *ApJ*, 159, 525
- Peters G. J., Polidan R. S., 1985, in Como, Italy, Hayes D. S., Pasinetti L.E., Davis Philip A.G., eds, *Proc. IAU Symp. 111, Calibration of fundamental stellar quantities*, p. 417
- Perryman M. A. C., et al, 1997, *A&A*, 323, L49
- Pintado O. I., Adelman S. J., 1993, *MNRAS*, 264, 63
- Pradhan A. K., Zhang H. L., Nahar S. N., Romano P., Bautista M. A., 1996, *A&AS*, 189, 7211
- Proffitt C. R., Quigley M. F., 2001, *ApJ*, 548, 429
- Reitermann A., Baschek B., Stahl O., Wolf B., 1990, *A&A*, 234, 109
- Rodríguez M., 2002, *A&A*, 389, 556
- Rolleston W. R. J., Trundle, C., Dufton P. L., 2002, *A&A*, 396, 53
- Rolleston W. R. J., Venn K., Tolstoy E., Dufton P. L., 2003, *A&A*, 400, 21
- Rubin R. H., et al., 1997, *ApJ*, 474, L131
- Ryans R. S. I., Dufton P. L., Rolleston W. R. J., Lennon D. J., Keenan F. P., Smoker J. V., Lambert D. L., 2002, *MNRAS*, 336, 577
- Ryans R. S. I., Dufton P. L., Mooney C. J., Rolleston W. R. J., Keenan F. P., Hubeny I., Lanz T., 2003, *A&A*, 401, 1119
- Schmidt E. G., Carruthers G. R., 1995, *ApJS*, 96, 605
- Sigut T. A. A., Pradhan A. K., 2003, *ApJS*, 145, 15
- Sigut T. A. A., Pradhan A. K., Nahar S. N., 2004, *ApJ*, 611, 81
- Smartt S. J., Dufton P. L., Lennon D. J., 1997, *A&A*, 326, 763
- Snijders M. A. J., 1969, *A&A*, 1, 452
- Swings J. P., Vreux J. M., 1976, *A&A*, 52, 161
- Thompson G. I., Humphries C. M., Nandy K., 1974, *ApJ*, 187, L81
- Thompson H. M. A., Keenan F. P., Dufton P. L., Ryans R. S. I., Smoker J. V., 2006, *MNRAS*, 368, 1749
- Thompson H. M. A., Keenan F. P., Dufton P. L., Ryans R. S. I., Smoker J. V., Lambert D. L., Zijlstra A. A., 2007, *MNRAS*, 378, 1619
- Trundle C., Dufton P. L., Lennon D. J., Smartt S. J., Urbaneja M. A., 2002, *A&A*, 395, 519
- Trundle C., Lennon D. J., Puls J., Dufton P. L., 2004, *A&A*, 417, 217
- Trundle C., Dufton P. L., Hunter I., Evans C. J., Lennon D. J., Smartt S. J., Ryans R. S. I., 2007, *A&A*, 471, 625
- Van Helden R., 1972, *A&AS*, 7, 311
- Van Helden R., 1972, *A&A*, 21, 209
- Zhang X.-G., Dultzin-Hacyan D., Wang T.-G., 2007, *RMxAA*, 43,101

Table 3. Fe III wavelengths and transitions, with atomic data taken from the Kurucz database^a (<http://nova.astro.umd.edu>, Hubeny 1988; Hubeny & Lanz 1995; Hubeny et al. 1998) and Nahar & Pradhan (1996)^b.

Wavelength (Å)	Transition ^b	g_i^b	g_j^b	Kurucz ^a log gf	N&P ^b log gf	Wavelength (Å)	Transition ^b	g_i^b	g_j^b	Kurucz ^a log gf	N&P ^b log gf
3953.76	$d^3G^e-w^3G^o$	9	9	-1.834	-2.153	4365.64	$a^5P^e-z^5P^o$	3	3	-3.404	-3.305
4005.04	$e^3F^e-z^3F^o$	9	9	-1.755	-1.810	4371.34	$a^5P^e-z^5P^o$	7	5	-2.992	-2.813
4022.11	$c^5F^e-t^5F^o$	9	9	-3.268	-3.438	4382.51	$a^5P^e-z^5P^o$	5	5	-3.018	-3.562
4022.35	$e^3F^e-z^3F^o$	7	7	-2.054	-1.967	4419.60	$a^5P^e-z^5P^o$	7	7	-1.690	-2.516
4035.43	$y^7P^o-c^7S^e$	5	7	0.119	0.147	4431.02	$a^5P^e-z^5P^o$	5	7	-2.572	-2.819
4039.16	$e^3F^e-z^3F^o$	5	5	-2.349	-2.091	4569.76	$d^1G^e-y^1G^o$	9	9	-1.870	-1.701
4053.11	$y^7P^o-c^7S^e$	7	7	0.261	0.291	5063.42	$b^5D^e-z^5P^o$	1	3	-2.950	-3.087
4053.47	$u^5F^o-g^5D^e$	3	5	-1.439	-1.273	5086.52	$w^5P^o-e^5D^e$	3	3	-1.307	-2.141
4081.01	$y^7P^o-c^7S^e$	9	7	0.364	0.398	5086.70	$b^5D^e-z^5P^o$	5	3	-2.590	-2.845
4122.03	$y^7P^o-b^7D^e$	5	5	0.436	0.431	5087.37	$b^5D^e-v^5P^o$	5	3	-0.733	-0.778
4122.78	$y^7P^o-b^7D^e$	5	3	0.364	0.386	5127.39	$b^5D^e-z^5P^o$	7	5	-2.218	-2.423
4123.00	$v^5P^o-c^5P^e$	7	5	0.051	0.041	5127.63	$b^5D^e-z^5P^o$	5	5	-2.564	-2.627
4137.01	$v^5P^o-c^5P^e$	7	5	0.051	0.041	5156.11	$b^5D^e-z^5P^o$	9	7	-2.018	-2.140
4137.13	$y^5H^o-b^5I^e$	7	9	0.719	0.808	5193.91	$b^5D^e-z^5P^o$	7	7	-2.852	-2.730
4137.76	$y^7P^o-b^7D^e$	7	9	0.644	0.658	5235.66	$a^7D^e-y^7P^o$	9	9	-0.107	-0.074
4139.35	$y^7P^o-b^7D^e$	7	7	0.553	0.547	5272.37	$a^7D^e-y^7P^o$	5	7	-0.421	-0.382
4140.48	$y^7P^o-b^7D^e$	7	5	0.114	0.128	5272.90	$b^5G^e-y^5H^o$	9	9	-0.409	-2.229
4154.96	$y^7P^o-b^7D^e$	11	13	0.891	0.964	5272.98	$a^5I^e-y^5H^o$	17	15	0.598	0.677
4164.73	$y^7P^o-b^7D^e$	9	11	0.935	0.946	5276.19	$d^3D^e-y^3D^o$	5	7	-7.667	-5.334
4164.92	$y^5H^o-b^5I^e$	13	15	1.011	1.042	5276.48	$a^7D^e-y^7P^o$	7	7	-0.001	0.036
4166.84	$y^7P^o-b^7D^e$	9	9	0.409	0.431	5282.30	$a^7D^e-y^7P^o$	9	7	0.108	0.146
4166.88	$y^5H^o-h^5G^e$	11	9	0.436	-0.587	5282.58	$d^3D^e-y^3D^o$	7	7	-3.648	-4.432
4220.12	$v^5D^o-g^5G^e$	7	9	-0.565	-0.347	5284.83	$a^5I^e-y^5H^o$	13	13	0.472	0.601
4222.27	$w^5P^o-d^5S^e$	7	5	0.272	0.153	5284.83	$a^5I^e-y^5H^o$	15	13	-0.836	-0.531
4238.62	$w^5P^o-d^5S^e$	5	5	-0.030	0.006	5299.93	$a^7D^e-y^7P^o$	3	5	-0.166	-0.129
4248.34	$v^5F^o-h^5G^e$	9	11	0.288	0.099	5302.60	$a^7D^e-y^7P^o$	5	5	-0.120	-0.083
4248.77	$w^5P^o-d^5S^e$	3	5	-0.095	-0.217	5306.13	$a^5I^e-y^5H^o$	9	9	-0.992	-0.706
4260.31	$v^5F^o-h^5G^e$	5	7	0.326	-0.168	5306.76	$c^5F^e-w^5D^o$	7	5	-0.341	-0.306
4261.39	$z^7F^o-a^7G^e$	3	5	0.251	-0.041	5375.47	$d^5G^e-u^5F^o$	13	11	0.461	0.543
4261.72	$v^5F^o-h^5G^e$	5	5	-0.918	-0.868	5375.57	$e^5G^e-w^5G^o$	9	7	-1.322	-0.904
4273.37	$z^7F^o-a^7G^e$	5	5	0.252	-0.077	5460.80	$d^3G^e-y^3H^o$	7	9	-1.519	-1.459
4273.41	$z^7F^o-a^7G^e$	5	7	0.498	0.169	5485.52	$d^3G^e-y^3H^o$	9	11	-1.469	-1.370
4286.09	$z^7F^o-a^7G^e$	7	5	-0.512	-0.874	5573.42	$d^3G^e-y^3H^o$	11	13	-1.390	-1.286
4286.13	$z^7F^o-a^7G^e$	7	7	0.374	0.012	5733.94	$b^7S^e-y^7P^o$	7	9	0.616	0.628
4286.16	$z^7F^o-a^7G^e$	7	9	0.705	0.343	5999.54	$c^3I^e-t^3H^o$	5	5	0.355	0.378
4296.81	$z^7F^o-a^7G^e$	9	7	-0.536	-0.921	6000.09	$e^3G^e-s^3G^o$	11	11	0.410	-0.862
4296.85	$z^7F^o-a^7G^e$	9	9	0.418	0.033	6032.60	$b^5S^e-w^5P^o$	5	7	0.497	0.521
4296.85	$z^7F^o-a^7G^e$	9	11	0.879	0.494	6032.67	$c^3I^e-x^3I^o$	13	15	0.410	-0.862
4304.79	$z^7F^o-a^7G^e$	11	11	0.377	-0.021	6035.52	$c^5G^e-x^5G^o$	13	11	-0.200	-0.463
4304.75	$z^7F^o-a^7G^e$	11	9	-0.699	-1.097	6036.55	$c^5G^e-x^5G^o$	13	13	0.790	0.684
4304.77	$z^7F^o-a^7G^e$	11	13	1.027	0.627						
4310.34	$z^7F^o-a^7G^e$	13	11	-1.072	-1.482						
4310.36	$z^7F^o-a^7G^e$	13	13	0.189	-0.217						
4310.36	$z^7F^o-a^7G^e$	13	15	1.156	0.747						
4352.58	$a^5P^e-z^5P^o$	5	3	-2.870	-2.827						